Glycobiology vol. 23 no. 12 pp. 1477–1490, 2013
doi:10.1093/glycob/cwt075
Advance Access publication on September 13, 2013

Bisected, complex N-glycans and galectins in mouse mammary tumor progression and human breast cancer

Hazuki E Miwa[2], Wade R Koba[3], Eugene J Fine[3], Orsi Giricz[4], Paraic A Kenny[4], and Pamela Stanley[1,2]

[2]Department of Cell Biology; [3]Department of Radiology, M. Donald Blaufox Laboratory for Molecular Imaging; and [4]Department of Developmental and Molecular Biology, Albert Einstein College of Medicine, New York, NY 10461, USA

Received on July 12, 2013; revised on August 23, 2013; accepted on September 4, 2013

Bisected, complex N-glycans on glycoproteins are generated by the glycosyltransferase MGAT3 and cause reduced cell surface binding of galectins. Previously, we showed that MGAT3 reduces growth factor signaling and retards mammary tumor progression driven by the Polyoma middle T antigen (PyMT) expressed in mammary epithelium under the mouse mammary tumor virus (MMTV) promoter. However, the penetrance of the tumor phenotype became variable in mixed FVB/N and C57BL/6 female mice and we therefore investigated a congenic C57BL/6 *Mgat3*$^{-/-}$/MMTV-PyMT model. In the absence of MGAT3, C57BL/6 *Mgat3*$^{-/-}$/MMTV-PyMT females exhibited accelerated tumor appearance and increased tumor burden, glucose uptake in tumors and lung metastasis. Nevertheless, activation of extracellular signal-regulated kinase (ERK)1/2 or protein kinase B (AKT) was reduced in ~20-week C57BL/6 MMTV-PyMT tumors lacking MGAT3. Activation of focal adhesion kinase (FAK), protein tyrosine kinase Src, and p38 mitogen-activated protein kinase were similar to that of controls. All the eight mouse galectin genes were expressed in mammary tumors and tumor epithelial cells (TECs), but galectin-2 and -12 were not detected by western analysis in tumors, and galectin-7 was not detected in 60% of the TEC lines. From microarray data reported for human breast cancers, at least 10 galectin and 7 N-glycan N-acetylglucosaminyl (GlcNAc)-transferase (MGAT) genes are expressed in tumor tissue, and expression often varies significantly between different breast cancer subtypes. Thus, in summary, while MGAT3 and bisected complex N-glycans retard mouse mammary tumor progression, genetic background may modify this effect; identification of key galectins that promote mammary tumor progression in mice is not straightforward because all the eight galectin genes are expressed; and high levels of MGAT3, galectin-4, -8, -10, -13 and -14 transcripts correlate with better relapse-free survival in human breast cancer.

Keywords: breast cancer / galectins / mammary tumors / MGAT3 / TCGA

Introduction

The functions of complex N-glycans attached to cell surface proteins range from modulating protein stability and turnover to mediating cell–cell or cell–matrix interactions via glycan-binding proteins, including galectins (Varki et al. 2009). Galectins bind to glycans that contain β-galactosides through carbohydrate recognition domains (CRDs) (Leffler et al. 2004; Di Lella et al. 2011). Galectins are synthesized in the cytoplasm, secreted via an unconventional pathway and then bound to the glycans of cell surface glycoproteins (Seelenmeyer et al. 2005; Seelenmeyer et al. 2008). Complex N-glycans offer multiple galectin-binding sites on (poly)N-acetyllactosamine (LacNAc) units ($[Gal\beta1,4GlcNAc]_n$) of their branches (Figure 1). Multivalency is a key feature of galectin binding, responsible for crosslinking multiple targets and forming a galectin–glycoprotein lattice on the cell surface (Brewer et al. 2002; Dennis and Brewer 2013). Prototypical galectins contain one CRD and typically dimerize to establish bivalency. In contrast, the tandem repeat subtype contains two distinctive CRDs per molecule and thus achieves bivalency without multimerization. Finally, the chimera type (galectin-3) forms a pentamer in the presence of ligands (Ahmad et al. 2004).

A galectin lattice has been implicated in tumor progression through modulation of growth factor signaling (Lau and Dennis 2008; Boscher et al. 2011). For example, galectin-3 is proposed to cluster glycosylated growth factor receptors on the cell surface and inhibit constitutive endocytosis, prolonging downstream signaling and thereby promoting cell proliferation and survival through enhanced extracellular signal-regulated kinase (ERK) and protein kinase B (AKT) pathways (Partridge et al. 2004; Lau et al. 2007). Galectin-1, on the other hand, contributes to immunosuppression and enhancement of angiogenesis, two key factors that promote tumor growth and metastasis (Thijssen et al. 2006; Thijssen et al. 2010; Banh et al. 2011; Dalotto-Moreno et al. 2013). In contrast, galectin-9 is believed to be antimetastatic by inhibiting tumor cell adhesion to vascular endothelium and extracellular matrices (Nobumoto et al. 2008). Therefore, it is important to determine the number of different galectins expressed in tumors in order to ascertain roles for galectins in tumor progression.

[1]To whom correspondence should be addressed: Tel: +1-718-430-3346; Fax: +1-718-430-8574; e-mail: pamela.stanley@einstein.yu.edu

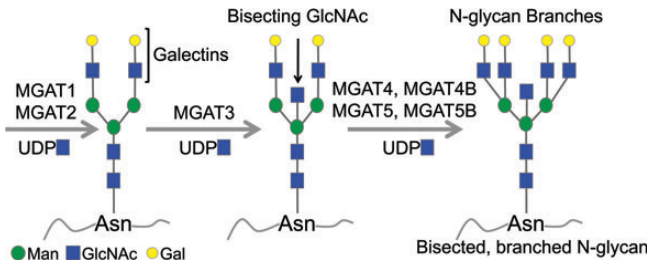

Fig. 1. Relationships between N-glycans, GlcNAc-transferases and galectins. MGAT1 and MGAT2 GlcNAc-transferases generate a biantennary, complex N-glycan. MGAT3 transfers GlcNAc from uridine diphosphate (UDP)-GlcNAc to the core mannose on a complex (or hybrid) N-glycan to generate a bisected, complex N-glycan. MGAT4A, MGAT4B, MGAT5 and MGAT5B add GlcNAc to generate branched, complex N-glycans. In Chinese hamster ovary (CHO) cells a Gal residue is added to each GlcNAc residue, except the bisecting GlcNAc (North et al. 2010). Each Gal may be extended by the addition of many (poly)LacNAc units ([Galβ1,4GlcNAc]$_n$). CHO mutant cells that express N-glycans with a bisecting GlcNAc (LEC10) exhibit reduced binding of ricin and galectin-1, -3 and -8, but increased binding of the lectin E-PHA compared with CHO cells that do not express MGAT3.

The bisecting GlcNAc is a unique N-glycan modification that occurs on complex or hybrid N-glycans following the action of β1,4-*N*-acetylglucosaminyltransferase III (GlcNAcT-III or MGAT3), encoded by the *Mgat3* gene (Figure 1). We have shown previously that the bisecting GlcNAc modulates plant lectin binding (Stanley et al. 1975; Campbell and Stanley 1984) and reduces the binding of galectin-1, -3 and -8 (Patnaik et al. 2006; Miwa et al. 2012). This is thought to be due to an effect of the bisecting GlcNAc on glycan conformation that reduces the accessibility of β-galactosides (Brisson and Carver 1983; Andre et al. 2004; Andre et al. 2007) and potentially due to a reduction in the numbers of Galβ1,4GlcNAc (LacNAc) units that are synthesized on N-glycans in the presence of the bisecting GlcNAc (North et al. 2010).

Previously, we reported the tumor suppressive roles of the bisecting GlcNAc and MGAT3 in the mouse mammary tumor virus Polyoma middle T antigen (MMTV-PyMT) model of mammary tumor formation (Song et al. 2010). Loss of MGAT3 from MMTV-PyMT tumor cells enhanced tumor progression and lung metastasis and increased growth factor signaling via ERK1/2. It remains to be determined whether the bisecting GlcNAc affects tumor growth via interactions with galectins, and if so, which galectins are most important. In this paper, we identify the galectins that are expressed in MMTV-PyMT mammary tumors and tumor cell lines and also in human breast cancers. During this work, the cohort of MMTV-PyMT females in the FVB/N and C57BL/6 (FVB/C57BL/6) mixed genetic background began to exhibit variable tumor latency in the absence of MGAT3. We, therefore, evaluated the effect of the *Mgat3* null mutation in a congenic C57BL/6 background. Here, we show that loss of MGAT3 in C57BL/6 MMTV-PyMT females promoted mammary tumor appearance, enhanced tumor burden, increased glucose uptake and promoted lung metastasis, as originally observed in the mixed genetic background (Song et al. 2010). In addition, analysis of galectin and N-glycan branching GlcNAc-transferase gene (*MGAT*) expression in data reported for different breast cancer subtypes by The Cancer Genome Atlas (TCGA) (Network CGA 2012) revealed complex expression patterns, some of which are prognostic for enhanced relapse-free survival (RFS).

Results

Genetic background affects mammary tumor formation in the absence of MGAT3

We previously reported that loss of MGAT3 and the bisecting GlcNAc on complex N-glycans enhances tumor progression in the mammary glands (MG) of *Mgat3*$^{-/-}$/MMTV-PyMT females (Song et al. 2010). In continuing studies however, we noticed that the time of tumor appearance in MG became highly variable in the FVB/C57BL/6 genetic background (Figure 2). This variability occurred in all *Mgat3* genotypes, resulting in no overall difference in the timing of palpable tumor appearance in *Mgat3* wild-type, heterozygotes and null females (Figure 2A–D). To reduce genetic heterogeneity, we investigated the model in a C57BL/6 background generated from MMTV-PyMT transgenic and *Mgat3*$^{+/-}$ mice that were both backcrossed to C57BL/6 >10 times. Mouse-to-mouse variability was less in the C57BL/6 background (Figure 2E–H). As observed previously (Song et al. 2010), the absence of MGAT3 accelerated tumor development and increased both tumor numbers and tumor mass at ~20 weeks (Figure 3A–C).

To determine if enhanced mammary tumor formation correlated with increased lung metastasis, lungs and lung sections from ~20-week C57BL/6 MMTV-PyMT females were examined for metastatic foci. Visible foci were rare at either the macro- or microscopic level and thus PyMT transcript levels were determined. Since MMTV-PyMT is expressed in mammary gland but not lung, the presence of PyMT transcripts in lung should reflect lung metastases. PyMT transcript levels were significantly higher in lungs from females lacking MGAT3 (Figure 3D).

Glucose uptake is increased in Mgat3$^{-/-}$ *mammary tumors*

Tumor cells increase glucose uptake and glycolysis to accommodate their rapid growth (Warburg et al. 1927; Gatenby and Gillies 2004). To determine whether *Mgat3*$^{-/-}$ mammary tumors took up more glucose than those expressing *Mgat3*, we used micro Positron Emission Tomography (microPET) to investigate regional glucose uptake in MMTV-PyMT-induced mammary tumors as described (Landskroner-Eiger et al. 2009). Mice of 16–17 and 19–20 weeks were analyzed after overnight fasting. Six mammary gland regions were selected as described in the Materials and methods section. Flattened three-dimensional (3D) views of representative images are shown with the six regions marked (Figure 4A). Consistent with a larger tumor burden, the maximum standardized-uptake value (SUV_{max}) of selected mammary gland regions of *Mgat3*$^{-/-}$ mice was significantly higher than control mice (Figure 4B). We have also analyzed the number of regions that had a SUV_{max} over the defined threshold value of 1 (above the whole body average) in each animal. These results showed that *Mgat3*$^{-/-}$ mice also had a larger number of mammary gland regions with high metabolic activity compared with wild-type (Figure 4C).

ERK and AKT activation were reduced in ~20-week mammary tumors lacking MGAT3

ERK and AKT activation have been implicated in cell proliferation and survival of MMTV-PyMT mammary tumor cells

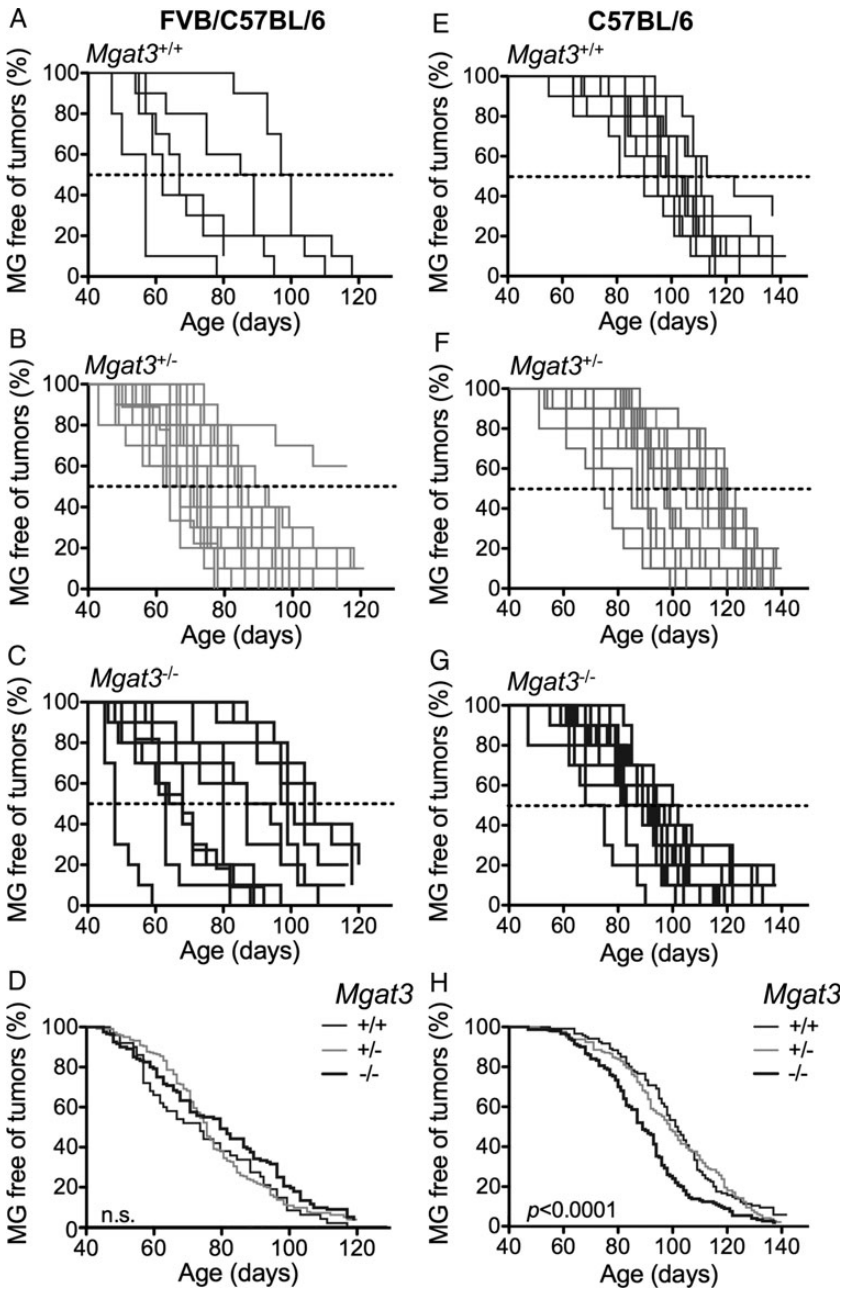

Fig. 2. Genetic background effects on MMTV-PyMT mammary tumor growth in the absence of MGAT3. KM plots of tumor-free MG vs. time for individual mice. (**A**–**C**) FVB/C57BL/6 mixed background *Mgat3*$^{+/+}$ ($n = 5$), *Mgat3*$^{+/-}$ ($n = 22$), *Mgat3*$^{-/-}$ ($n = 12$). (**D**) Combined MG free of tumors with time in the FVB/C57BL/6 background for all mice shown in (A–C). Not significant, log-rank (Mantel–Cox) test. (**E**–**G**) C57BL/6 congenic background *Mgat3*$^{+/+}$ ($n = 12$), *Mgat3*$^{+/-}$ ($n = 21$), *Mgat3*$^{-/-}$ ($n = 15$). (**H**) Combined MG free of tumors with time in the C57BL/6 background for mice shown in E and G. *Mgat3*$^{-/-}$ MG differ significantly from *Mgat3*$^{+/+}$ and *Mgat3*$^{+/-}$, $P < 0.0001$, log-rank (Mantel–Cox) test.

(Partridge et al. 2004; Williams et al. 2004; Iyengar et al. 2005). We previously showed that loss of MGAT3 in cultured cells and in MMTV-PyMT mammary tumors correlates with increased ERK1/2 phosphorylation (Song et al. 2010). Thus, we investigated ERK1/2 and AKT phosphorylation in tumor lysates from ~20-week C57BL/6/MMTV-PyMT females. The average sizes of selected tumors (*Mgat3*$^{+/+}$ 0.08 ± 0.03 g; *Mgat3*$^{-/-}$ 0.16 ± 0.04 g, mean ± standard deviation) were close to the median value of the four largest tumors from each genotype (*Mgat3*$^{+/+}$ 0.06 g, $n = 11$; *Mgat3*$^{-/-}$ 0.16 g, $n = 13$; $P < 0.0001$, Mann–Whitney test). The presence of the bisecting GlcNAc on *Mgat3*$^{+/+}$ tumor glycoproteins was demonstrated by enhanced binding of *Phaseolus vulgaris* erythroagglutinin (E-PHA) lectin compared with *Mgat3*$^{-/-}$ tumor glycoproteins (Figure 5A). In contrast, binding of *Phaseolus vulgaris* leukoagglutinin (L-PHA) or *Datura stramonium* agglutinin (DSA) lectins, which preferentially bind to β1,6-branched and (poly)LacNAc-containing N-glycans, respectively, was indistinguishable between the

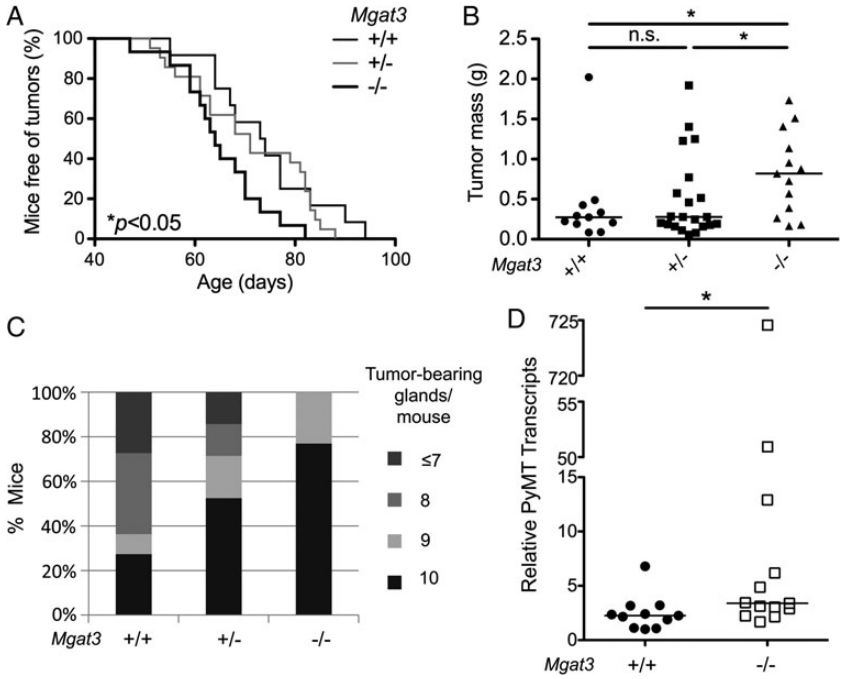

Fig. 3. Loss of MGAT3 accelerates tumor progression in C57BL/6 MMTV-PyMT females. (**A**) Mice free of tumors over time in the C57BL/6 background ($Mgat3^{+/+}$ ($n = 12$), $Mgat3^{+/-}$ ($n = 21$), $Mgat3^{-/-}$ ($n = 15$)). $Mgat3^{-/-}$ females were significantly different from $Mgat3^{+/+}$ and $Mgat3^{+/-}$, $P < 0.05$, log-rank (Mantel–Cox) test. (**B**) Combined mass of three largest tumors from ~20-week C57BL/6/PyMT mice ($Mgat3^{+/+}$ ($n = 11$), $Mgat3^{+/-}$ ($n = 21$), $Mgat3^{-/-}$ ($n = 13$)). Bar indicates the median, $^*P < 0.05$, nonparametric Mann–Whitney test. (**C**) 100% stacked bar graph comparing the relative population of ~20-week C57BL/6/MMTV-PyMT mice with respective number of MG with solid tumors typically ≥10 mm^3 ($Mgat3^{+/+}$ ($n = 11$), $Mgat3^{+/-}$ ($n = 21$), $Mgat3^{-/-}$ ($n = 13$)). (**D**) Quantitative real-time PCR was used to determine the relative PyMT/β-actin transcript levels in total RNA from lungs of $Mgat3^{+/+}$ ($n = 11$) and $Mgat3^{-/-}$ ($n = 13$) females. Graph represents the fold-change of each sample against the control sample (see Materials and methods section). Bar indicates the median ($^*P < 0.05$, Mann–Whitney test).

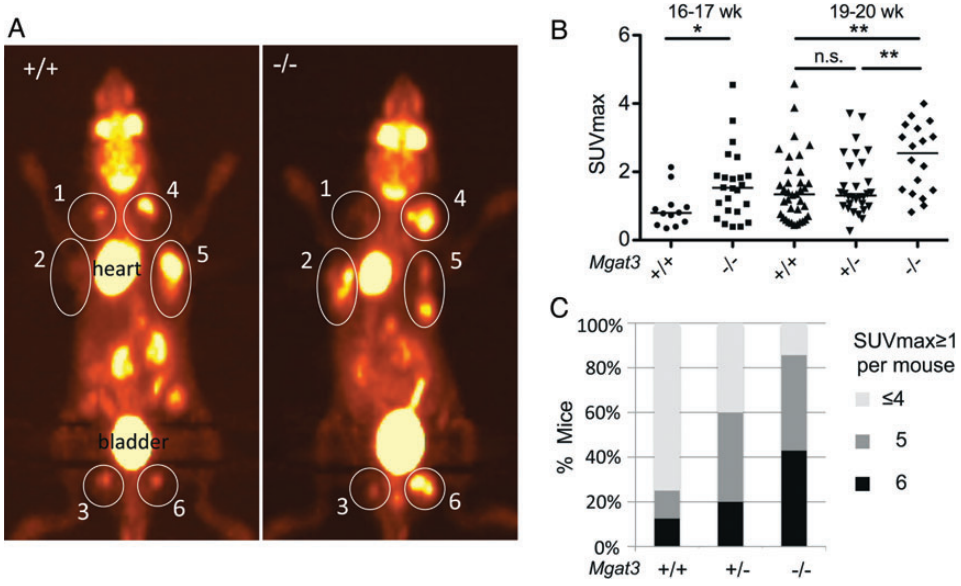

Fig. 4. Glucose analog uptake is increased in $Mgat3^{-/-}$ mammary tumors. (**A**) SUV_{max} was measured in six ROI per mouse. Representative flattened projection 3D images of a dorsal view of $Mgat3^{+/+}$ and $Mgat3^{-/-}$ littermates are shown. (**B**) SUV_{max} of six mammary gland regions per mouse (16–17 weeks: $Mgat3^{+/+}$ ($n = 2$), $Mgat3^{-/-}$ ($n = 4$), 19–20 weeks: $Mgat3^{+/+}$ ($n = 6$), $Mgat3^{+/-}$ ($n = 5$), $Mgat3^{-/-}$ ($n = 3$)). Bar indicates the median ($^*P < 0.05$, $^{**}P < 0.01$, Mann–Whitney test). (**C**) 100% stacked bar graph comparing the relative population of mice with mammary gland regions having SUV_{max} >1. Data frommice of 16–17 and 19–20 weeks were combined ($Mgat3^{+/+}$ ($n = 8$), $Mgat3^{+/-}$ ($n = 5$) and $Mgat3^{-/-}$ ($n = 7$)).

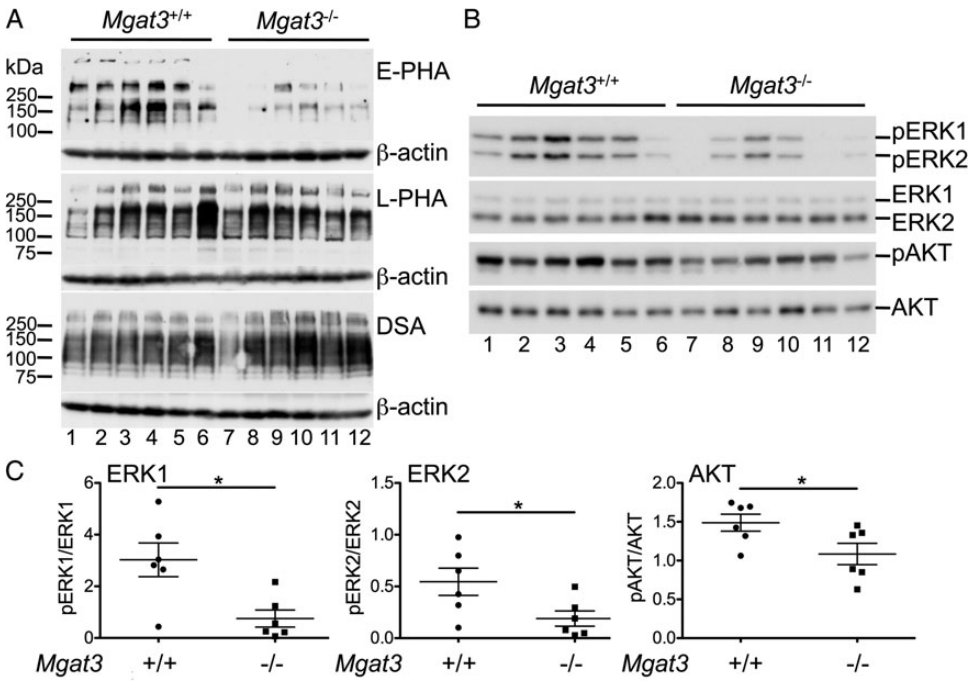

Fig. 5. ERK and AKT activation are reduced in mammary tumors of ~20-week *Mgat3*$^{-/-}$MMTV-PyMT mice. (**A**) Tumor lysates (80 μg protein) from *Mgat3*$^{+/+}$ MMTV-PyMT (lanes 1–6) or *Mgat3*$^{-/-}$MMTV-PyMT (lanes 7–12) mammary tumors were separated on 10% SDS–PAGE gels, and transferred to PVDF membranes were probed with biotinylated E-PHA, L-PHA or DSA lectin. β-actin was a loading control. (**B**) Western blot analysis of tumor lysates (40 μg) from *Mgat3*$^{+/+}$ MMTV-PyMT (lanes 1–6) and *Mgat3*$^{-/-}$MMTV-PyMT (lanes 7–12) C57BL/6 females to detect pERK1/2, ERK1/2, pAKT (Ser473) and AKT. (**C**) Relative band intensity was determined by the NIH ImageJ software. Ratios of pERK1/ERK1, pERK2/ERK2 and pAKT/AKT are shown. Bars are mean ± standard error of mean (SEM) ($n = 6$ tumors from six mice per genotype). *, $P < 0.05$, two-tailed Student's t test. Data are representative of a replicate experiment.

two genotypes (Figure 5A). Unexpectedly, phosphorylation of both ERK1/2 and AKT were reduced in *Mgat3*$^{-/-}$ compared with wild-type tumor lysates (Figure 5B and C). In contrast, activation of p38 mitogen-activated protein kinase (p38MAPK), Src and focal adhesion kinase (FAK) in the same tumor lysates was not significantly different between *Mgat3*$^{+/+}$ and *Mgat3*$^{-/-}$ tumors (data not shown). Acute ERK1 activation in response to epidermal growth factor (EGF) stimulation was enhanced in one *Mgat3* null tumor epithelial cell (TEC) line compared with controls (Figure 6A and C). In addition, the deactivation of ERK1/2, assessed by the level of phosphorylated ERK1/2 at 10 min post-EGF stimulation, was delayed in both *Mgat3*$^{-/-}$ TECs (Figure 6A and C), indicating prolonged growth factor signaling in the absence of MGAT3, reflected by their reduced E-PHA signal (Figure 6B). Thus, *Mgat3*$^{-/-}$ cultured TECs responded somewhat better than wild-type to EGF stimulation. However, the data from tumor lysates suggest that *Mgat3*$^{-/-}$/MMTV-PyMT tumors had reached a point of reduced growth factor signaling via ERK1/2 or AKT, compared with their *Mgat3*$^{+/+}$ counterparts by ~20 weeks. In contrast, at a similar stage of tumor progression, *Mgat3*$^{-/-}$/MMTV-PyMT FVB/C57BL/6 tumors and TECs exhibited enhanced ERK1/2 activation (Song et al. 2010).

MMTV-PyMT mammary tumors and TECs express eight galectin genes

The bisecting GlcNAc transferred by MGAT3 is a significant modulator of galectin binding to glycoproteins (Andre et al. 2004; Patnaik et al. 2006; Andre et al. 2007; Miwa et al. 2012). Up to 15 galectins have been identified, including 11 in human and 8 in mice (9 in some strains (Houzelstein et al. 2008)). Whereas galectin-3 has been implicated as a cross-linker of complex N-glycans that prolongs growth factor signaling and enhances mammary tumor progression in the MMTV-PyMT model (Partridge et al. 2004; Lau et al. 2007), the deletion of galectin-3 has no effect on mammary tumor progression in MMTV-PyMT tumors (Eude-Le Parco et al. 2009). We, therefore, investigated the range of galectin genes (*Lgals*) expressed in mouse MMTV-PYMT mammary tumors. Reverse transcription–polymerase chain reaction (RT–PCR) was performed on total RNA harvested from three independent tumors per genotype using the primer sets given in Supplementary data Table SII. PCR products were initially confirmed by sequencing. *Mgat3* transcripts were present in RNA from *Mgat3*$^{+/+}$ but not *Mgat3*$^{-/-}$ tumors, while transcripts of PyMT and *Mgat5*, which encode a distinct branching glycosyltransferase (Figure 1), were similar in all tumors (Figure 7A). Interestingly, transcripts from all the eight mouse galectin genes were detected in MMTV-PyMT mammary tumors (Figure 7A). While most galectins were also detected by western analysis, galectin-2 and -12 were not, although bands of the expected molecular weight were obtained in control tissues (Figure 7B). Similar results were obtained by RT–PCR of cDNA from mammary tumors of FVB/C57BL/6-MMTV-PyMT females (data not shown).

Because tumor tissue is composed of a heterogeneous mixture including tumor cells, immune cells and adipocytes, we also investigated the galectins expressed in cultured TEC

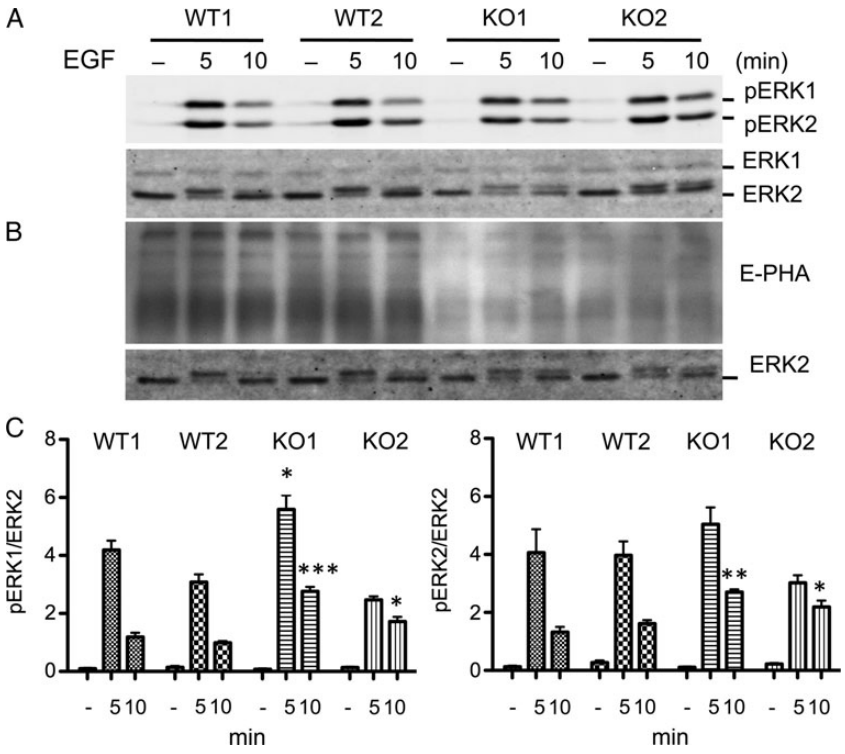

Fig. 6. EGF signaling in MMTV-PyMT TECs. EGF signaling in independent *Mgat3*$^{+/+}$MMTV-PyMT (WT1 and WT2) and *Mgat3*$^{-/-}$MMTV-PyMT (KO1 and KO2) TECs. (**A**) Representative blots for pERK1/2 and total ERK1/2. (**B**) Representative E-PHA lectin and ERK2 (loading control) blots. (**C**) Histogram of pERK1 and pERK2 over total ERK2 (both bands). Mean ± SEM from three independent experiments. Statistical significance for WT1 or WT2 vs. KO1 and WT1 or WT2 vs. KO2 determined by one way analysis of variance, Newman–Keuls multiple comparison test, *$P < 0.05$, ** $P < 0.01$ and *** $P < 0.001$.

lines to determine galectins intrinsic to the tumor cells. *Mgat3* transcripts and E-PHA and L-PHA-binding glycoproteins were present in *Mgat3*$^{+/+}$ but not *Mgat3*$^{-/-}$ TECs, while transcripts of *Mgat5* were similar in *Mgat3*$^{+/+}$ and *Mgat3*$^{-/-}$ TECs (Figure 8A and B). Although, PyMT expression was higher in *Mgat3*$^{-/-}$ TECs (Figure 8A), such differences were not observed in tumors (Figure 7A), or in comparisons of 3 *Mgat3*$^{+/+}$ and 3 *Mgat3*$^{-/-}$ TEC lines generated from mammary tumors of FVB/C57BL/6 females (data not shown), nor in TEC lines developed previously (Song et al. 2010). Importantly, all the eight galectin genes were expressed in *Mgat3*$^{+/+}$ and *Mgat3*$^{-/-}$TECs (Figure 8A). Western analyses showed that galectin-2 and -12 were not detected, as observed for tumor tissue, and galectin-7 was detected only in one of the four cell lines (Figure 8B). Since galectin-7 was readily detected in western blots of all tumor tissues, the fact that most TECs have no detectable galectin-7 protein suggests that it is mainly expressed in stromal cells of the tumor. Galectin-4 and -8 protein isoforms were observed in both tumors and TECs. However, the prominent bands in galectin-8 blots were different between tumors and TECs (42 vs. 45 kDa). We also noted for galectin-9 that tumor tissues contained predominantly an ∼36 kDa species, but an ∼45 kDa species was more prominent in TECs. Similar results were obtained following western analyses of TEC lines derived from FVB/C57BL/6-MMTV-PyMT tumors—galectin-2 and -12 were not detected, and galectin-7 was detected only in three of six FVB/C57BL/6 TEC lines (data not shown). In conclusion, galectins-1, -3, -4, -8 and -9 were the galectins most robustly expressed at both transcript and protein levels in tumor tissues and TECs. However, all the eight mouse galectin genes were expressed in TECs, and thus the full range of galectins may influence tumor progression in the MMTV-PyMT mammary tumor model.

Galectins and complex N-glycans in human breast cancer

In order to develop mouse models that may provide insights into roles for galectins and the glycosyltransferases responsible for the synthesis of complex N-glycans in human breast cancer, we analyzed published microarray data reported by TCGA for various cohorts of women with breast cancers of different subtypes (Network CGA 2012). The expression data are presented as a heat map with statistically significant differences between breast tumor subtypes shown in an adjacent table (Figure 9). Among the galectins, basal-like breast cancer (BLBC) differed from each of the other types, having increased galectin-2 and -7 expression but decreased galectin-8 expression, compared with overall median expression levels. Compared with Luminal A, BLBC differed in the expression of two additional galectins, galectin-9 and -12. Compared with Luminal B, expression of galectin-2, -4, -7 and -8 were significantly different in BLBC. Galectin-3 expression was significantly lower in Luminal B than in human epidermal growth factor receptor 2 (HER2) and Luminal A tumors. In general, galectin-2, -7, -8 and -12 exhibited the most variation in expression. Among the glycosyltransferase genes that generate complex N-glycans, multiple

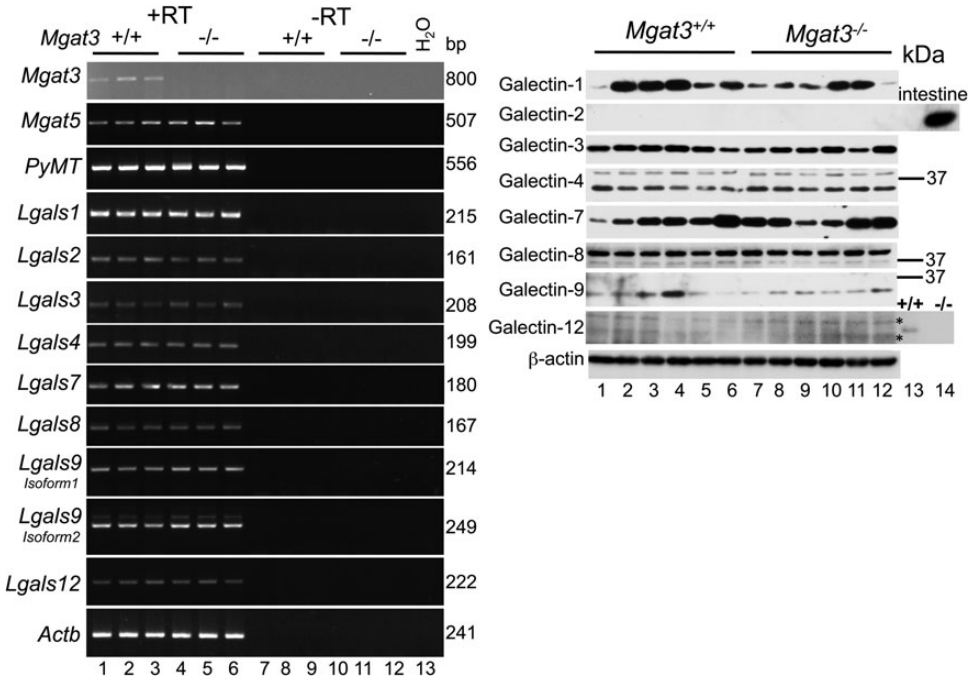

Fig. 7. Galectin expression in MMTV-PyMT mammary tumors. (**A**) The expression of the eight known mouse galectins, including two galectin-9 splice isoforms/variants, were analyzed by RT–PCR using cDNA prepared from total RNA of 3 *Mgat3*$^{+/+}$ (lanes 1–3) and 3 *Mgat3*$^{-/-}$ (lanes 4–6) MMTV-PyMT mammary tumors. Reactions lacking RT (-RT; lanes 7–12) or cDNA (H_2O; lane 13). The expression of *Mgat3*, *Mgat5*, PyMT and *Acbt* (β-actin) are also shown. Primer sets for *Lgals9* variant 2 generate PCR products from both variant 2 (major band at 249 bp) and variant 1 (minor band at 342 bp). (**B**) Six *Mgat3*$^{+/+}$ and six *Mgat3*$^{-/-}$ MMTV-PyMT mammary tumor lysates (20 µg protein (galectin-1 and -3) or 40 µg protein (all others) were loaded on 10% (galectin-9), 12% (galectin-3, -4, -8 and -12) or 15% (galectin-1, -2 and -7) SDS–PAGE gels with molecular weight markers. Separate blots were probed with antibodies against galectin-1 (∼14 kDa), galectin-2 (∼14 kDa), galectin-3 (∼30 kDa), galectin-4 (∼34 and ∼40 kDa), galectin-7 (∼14 kDa), galectin-8 (∼37 and ∼42 kDa), galectin-9 (∼34 kDa) and galectin-12 (∼34 kDa). In the galectin-2 blot, mouse small intestine lysate (2 µg) was a positive control (lane 14). In the galectin-12 blot, adipose tissue lysates (∼15 µg) from *Lgals12*$^{+/+}$ and *Lgals12*$^{-/-}$ mice (Yang et al. 2011) were positive and negative controls, respectively (lanes 13 and 14). The β-actin blot shown is representative of the β-actin blot performed with each galectin blot. Bands marked with asterisks indicate nonspecific bands.

expression differences were observed between BLBC and HER2 (*MGAT3*, *MGAT4A* and *MGAT5*), BLBC and Luminal A (*MGAT3*, *MGAT4A*, *MGAT4B*, *MGAT5* and *MGAT5B*) and BLBC and Luminal B (*MGAT2*, *MGAT3*, *MGAT4A* and *MGAT5*). Compared with the overall average, BLBC cancers have markedly increased expression of *MGAT3* and decreased expression of *MGAT4A*. Based on mouse studies, increased bisected N-glycans caused by *MGAT3* and reduced branched N-glycans due to reduced *MGAT4A* would be expected to retard tumor progression (Lau and Dennis 2008; Song et al. 2010; Miwa et al. 2012); this work). HER2-amplified tumors exhibit increased expression of *MGAT4A* and *MGAT5B*, which should both increase complex N-glycan branching and enhance tumor progression (Lau and Dennis 2008). Luminal A cancers have no differences from the overall average, and Luminal B only one difference in reduced expression of *MGAT3* which should enhance tumor progression.

Investigations of *LGALS* and *MGAT* genes in the breast cancer database Kaplan–Meier (KM) plotter (Gyorffy et al. 2010) showed that in data from all types of breast cancer ($n = 2978$), higher expression of *MGAT3* correlates with better RFS (hazard ratio (HR) < 1; Table I), as expected from mouse models (Song et al. 2010; Miwa et al. 2012); this work). Expression of *MGAT5* does not correlate with worse RFS, contrary to expectations from mouse models (Partridge et al. 2004; Lau et al. 2007; Guo et al. 2012). However, higher expression of *MGAT2* correlates with worse RFS (Table I), and this should lead to increased substrate for *MGAT5*, thereby enhancing N-glycan branching by an alternative mechanism to upregulation of *MGAT5*. With respect to *LGALS* transcripts, patients with higher expression of *LGALS4, LGALS8*, *LGALS10, LGALS13* and *LGALS14* have better RFS (Table I). Other galectins that correlate positively with RFS are *LGALS2* and *LGALS9*, whereas higher *LGALS1* expression correlates with worse RFS (HR > 1; Table I). From these data, it seems that augmenting *MGAT3* and galectin-4, -8, -10, -13 and -14 and reducing *MGAT2* and galectin-1 would be beneficial to breast cancer patients.

Discussion

In C57BL/6 MMTV-PyMT/*Mgat3*$^{-/-}$ females, the absence of MGAT3 and the bisecting GlcNAc on N-glycans enhanced tumor progression and lung metastasis as we observed initially (Song et al. 2010), though the effect became variable in the mixed genetic background, as reported here. Others have observed similar genetic background effects. For example, tumor progression and lung metastasis of MMTV-PyMT mice deficient in inducible nitric oxide synthase is significantly reduced in the congenic C57BL/6 background, but not in the

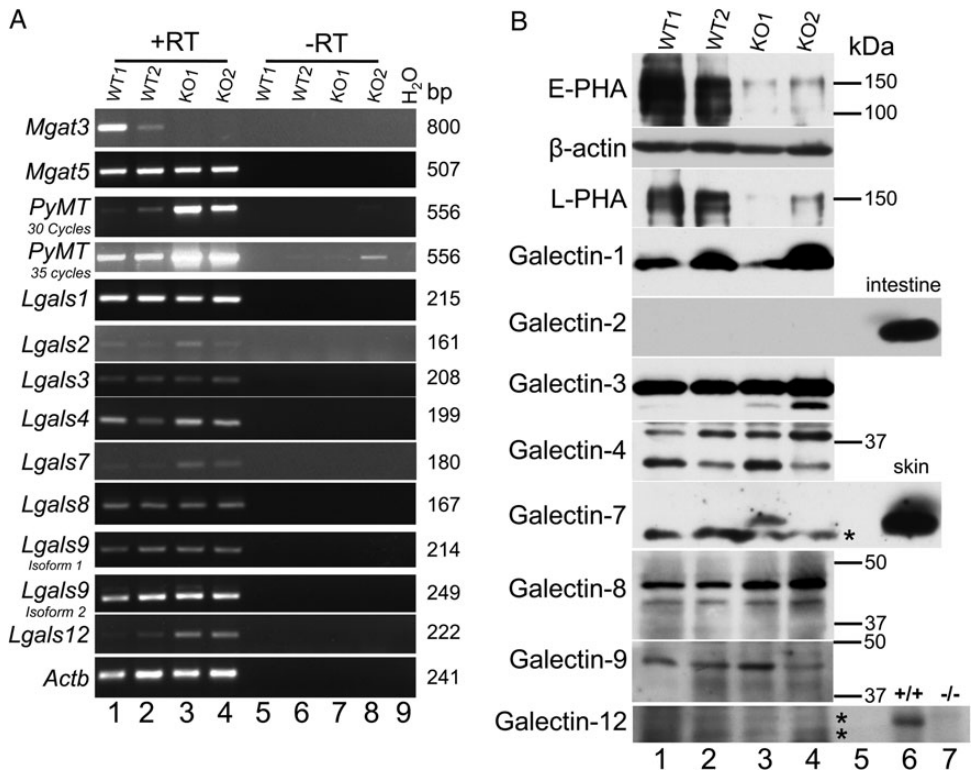

Fig. 8. Galectin expression in cultured TECs. (**A**) The expression of eight galectin genes (two galectin-9 isoforms/variants) along with *Mgat3*, *Mgat5*, PyMT and *Actb* were analyzed by RT–PCR using cDNA prepared from total RNA of wild-type $Mgat3^{+/+}$ (WT1 and WT2; lanes 1 and 2) and $Mgat3^{-/-}$ (KO1 and KO2; lanes 3 and 4) MMTV-PyMT TECs. Reactions lacking RT (-RT; lanes 5–8) or cDNA (H_2O; lane 9). (**B**) $Mgat3^{+/+}$ (WT1 and WT2; lanes 1 and 2) and $Mgat3^{-/-}$ (KO1 and KO2; lanes 3 and 4) TEC lysates containing 10 μg (galectin-1 and -3) or 40 μg (all the others) protein were separated on 10% (E-PHA, L-PHA, β-actin), 12% (galectin-3, -4, -8, -9 and -12) or 15% (galectin-1, -2 and -7) SDS–PAGE gels. Blots were separately probed with E-PHA, L-PHA or with antibodies against galectins as described in the legend to Figure 7. In the galectin-7 blot, skin lysate (40 μg) was a positive control. Galectin-2 and -12 controls are described in the Figure 7 legend. The β-actin blot is from the same membrane used for the E-PHA lectin blot and is representative of each experiment. Asterisks indicate nonspecific bands.

FVB/N background (Davie et al. 2007). Similarly, Lipocalin-2 null mice show reduced tumorigenesis in the C57BL/6 background (Berger et al. 2010), but not in the FVB/N background (Cramer et al. 2012). We also uncovered differences with respect to growth factor signaling and genetic background. Thus, while EGF- or platelet-derived growth factor-AB-induced ERK activation was reduced by the presence of MGAT3 and the bisecting GlcNAc in Chinese hamster ovary cells and TECs isolated from FVB/C57BL/6 MMTV-PyMT tumors (Song et al. 2010), the opposite effect was found in C57BL/6 mammary tumors examined at an equivalent time of tumor development (Figure 5). In the absence of MGAT3, ERK1/2 and AKT activation in tumor lysates were reduced, rather than enhanced, compared with control lysates. The levels of activated p38MAPK, Src and FAK were no different between wild-type mice and *Mgat3* null tumors. However, in $Mgat3^{-/-}$ TECs, the levels of phosphorylated ERK1/2 induced by EGF were maintained slightly longer compared with controls. Therefore, it appears that the underlying mechanism by which mammary tumorigenesis is increased in C57BL/6 $Mgat3^{-/-}$ mice is not simply due to increased signaling via a predominant growth factor signaling pathway. While the $Mgat3^{+/+}$ TEC lines examined here expressed fewer PyMT transcripts than the $Mgat3^{-/-}$ TEC lines (Figure 8A), such differences were not observed in other comparisons of TEC lines, nor in MMTV-PyMT tumors excised from control vs. *Mgat3* null mice.

microPET analysis revealed that $Mgat3^{-/-}$ tumors exhibited greater glucose uptake than $Mgat3^{+/+}$ tumors. In mouse mammary tumor cells, glucose uptake is mediated predominantly by glucose transporter 1 (GLUT1) as reduction of GLUT1 expression caused reduced glucose usage and tumor cell growth (Young et al. 2011). Increases in the number of N-acetyllactosamine (LacNAc) repeats in the N-glycan on GLUT1 have been observed in tumor cells (Kitagawa et al. 1995), which could be due to increased glucose metabolism leading to increased uridine diphosphate-GlcNAc levels (Ying et al. 2012) and thereby, increases in N-glycan branching and LacNAc repeats (Lau et al. 2007). Similarly, cell surface expression of GLUT2 and GLUT4 are regulated by N-glycans (Ohtsubo et al. 2005; Lau et al. 2007; Haga et al. 2011), and a critical role of the galectin lattice has been demonstrated for GLUT2 cell surface expression. Thus, the presence of the bisecting GlcNAc on the N-glycans of GLUT1 in mammary tumor cells may lower glucose uptake by reducing the amount of GLUT1 associated with a galectin lattice at the cell surface.

In order to investigate roles for galectins on the effects of MGAT3 and other branching GlcNAc-transferases in mammary tumor progression, we determined their expression in MMTV-PyMT mouse mammary tumors and cultured TECs.

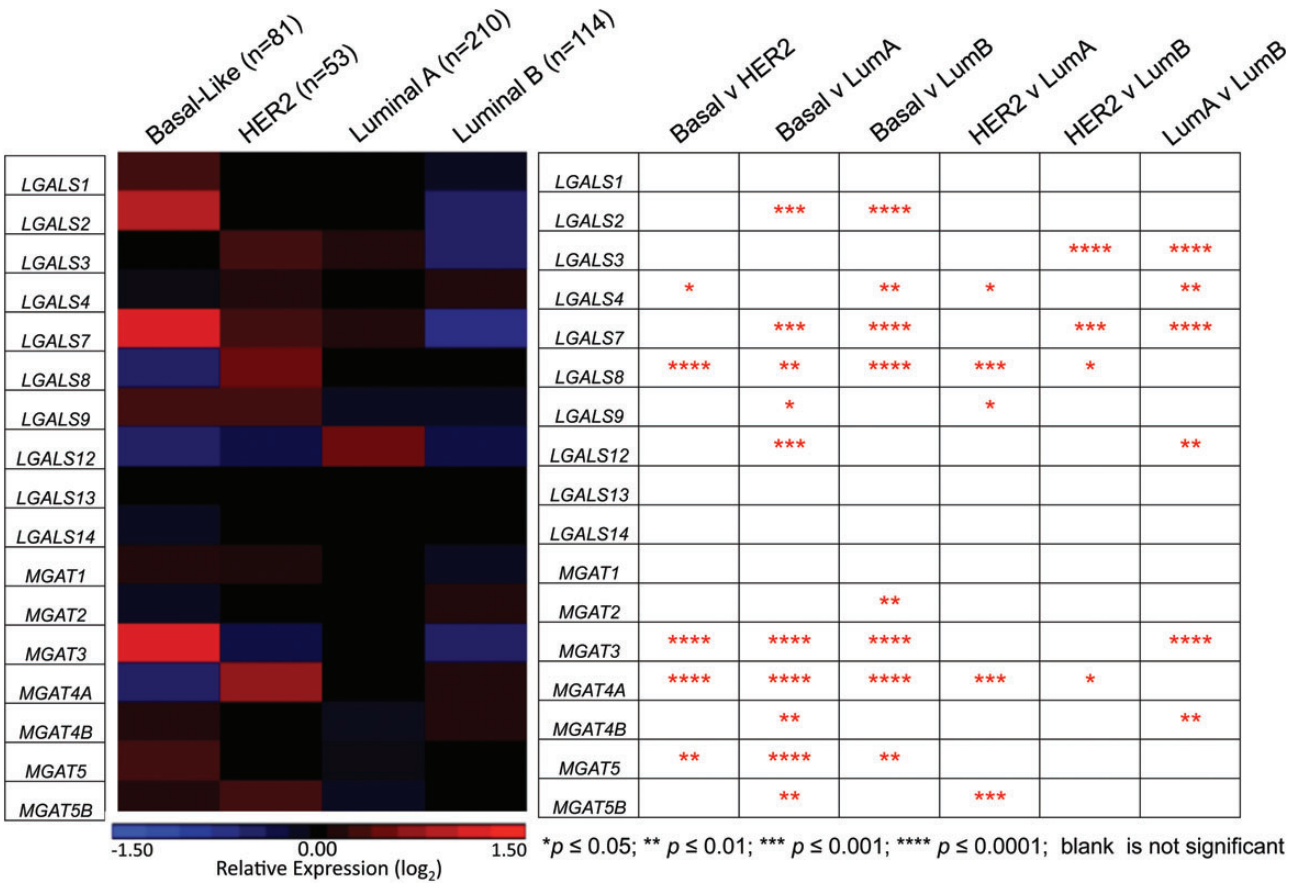

Fig. 9. *LGALS* and *MGAT* genes in human breast cancers. Expression of genes encoding galectins (*LGALS*) and N-glycan branching GlcNAc-transferases (*MGAT*) were analyzed in gene expression microarray data from 458 breast tumors in the TCGA study (Network CGA 2012). The heat map represents the fold-change between the median expression level of that gene in a given breast cancer subtype compared with the median expression level of that gene across all samples (log_2 scale). All of the data were used to test for significant differences between the median expression levels for each gene in each subtype (Kruskal–Wallis test with Dunn's posttest). Statistically significant *P*-values are indicated by asterisks in the adjacent table.

Table I. *LGALS* and *MGAT* genes and human breast cancer RFS

Gene	HR	95% confidence interval	*P*-value
LGALS1	1.23	1.08–1.39	**
LGALS2	0.85	0.75–0.96	**
LGALS3	1.12	0.99–1.27	
LGALS4	0.66	0.58–0.75	****
LGALS7	0.99	0.87–1.12	
LGALS8	0.67	0.59–0.76	****
LGALS9	0.87	0.77–0.99	*
LGALS10	0.72	0.63–0.82	****
LGALS13	0.68	0.60–0.77	****
LGALS14	0.65	0.57–0.74	****
MGAT1	0.95	0.84–1.07	
MGAT2	1.35	1.19–1.53	****
MGAT3	0.88	0.78–1.00	*
MGAT4A	0.9	0.79–1.02	
MGAT4B	1.15	1.02–1.31	*
MGAT5	1.08	0.95–1.22	

*$P \leq 0.05$; **$P \leq 0.01$; ***$P \leq 0.001$ and ****$P \leq 0.0001$.

Based on RT–PCR analysis, tumors and TECs express all the eight mouse galectin genes. According to western blot analyses, galectin-1, -3, -4, -7, - 8 and -9 were detected in tumor lysates and galectin-1, -3, -4, -8 and -9 in TECs. Galectin-7 may, therefore, be a component of the stromal microenvironment, which is known to influence tumor progression (Joyce and Pollard 2009). Clearly, however, a number of galectins may play roles in mammary tumor progression and some may share overlapping roles. Thus, removal of galectin-3 does not alter mammary tumor progression in a MMTV-PyMT mouse model (Eude-Le Parco et al. 2009), despite compelling evidence suggesting a major involvement of galectin-3 in promoting tumor growth and metastasis (Partridge et al. 2004; Dennis et al. 2009). It would be interesting to know whether other galectins are upregulated in galectin-3 null mammary tumors or TECs (Eude-Le Parco et al. 2009).

Galectins may regulate tumor cell growth and metastasis not only through regulation of growth factor and cytokine signaling, but also by promoting angiogenesis and immunosuppression, as shown for galectin-1 (Thijssen et al. 2006; Thijssen et al. 2010; Banh et al. 2011; Dalotto-Moreno et al. 2013). Thus, disruption of galectin-1 and N-glycan interactions suppresses hypoxia-induced angiogenesis and tumorigenesis in Kaposi's sarcoma (Croci et al. 2012). On the other hand, not all members of the galectin family act to promote tumorigenesis. In stark contrast to galectin-1 and -3, galectin-9 is proposed to

inhibit metastasis in human breast cancer, through blocking adhesion to endothelium and extracellular matrices (Irie et al. 2005; Nobumoto et al. 2008). Consistent with such reports, investigation of the data from 286 samples of invasive breast tumors (Wang et al. 2005) showed that high levels of galectin-2 and -9 expression correlated with lower recurrence of distant metastasis in patients with node-negative breast cancer. The expression of other galectins, including galectin-3, or *MGAT3*, *MGAT5* and the other branching GlcNAc-transferase genes did not indicate prognostic value from the same data (Wang et al. 2005). In contrast, investigation of the data of 295 breast cancer patients of the Netherlands Cancer Institute (NKI-295) (van de Vijver et al. 2002; van de Vijver 2005) indicated that high levels of galectin-9 correlate with poor survival. Interestingly, however, estrogen receptor (ER) negative status appears to correlate with higher levels of galectin-9 and thus, when survival was compared within a group with the same ER status (i.e. positive or negative), no correlation was detected. Clearly, the situation is complex given the changes in expression levels determined from the most recent TCGA data (Network CGA 2012) of several *LGALS* and *MGAT* genes in different breast cancer subtypes (Figure 9). In addition, based on microarray data in KM plotter, the increased expression of several galectin and *MGAT* genes correlates with RFS in breast cancer patients (Table I). Thus, reducing expression of galectin-1 and *MGAT2* and enhancing expression of *MGAT3* and galectins -4, -8, -10, -13 and -14 may potentially be beneficial to breast cancer patients. However, the molecular mechanisms underlying human breast tumor biology are complex, and with the likelihood of functional redundancy, it will be a challenge to ascertain roles for individual galectins *in vivo*. On the other hand, with the caveat that galectin expression may differ between humans and mice, predictions could be tested by generating mouse models using the efficient CRISPR/Cas method of genomic engineering (Wang et al. 2013) to conditionally delete multiple galectin genes in mammary epithelial or stromal cells.

Materials and methods

Mice

Mgat3$^{+/-}$ or *Mgat3*$^{-/-}$ mice (*Mgat3*^{tm1Jxm}) (Priatel et al. 1997) backcrossed >10 generations to C57BL/6 mice were mated with MMTV-PyMT transgenic male mice in the FVB/N (FVB) background (line #634) (Guy et al. 1992) (a gift from Dr. Jeffery Pollard, Albert Einstein College of Medicine, Bronx, NY) or the C57BL/6 background (Basu et al. 2004) (a gift from Dr. Sandra Gendler, Mayo Clinic, Rochester, MN). *Mgat3*$^{+/-}$ or *Mgat3*$^{-/-}$ females in the C57BL/6 background were mated with *Mgat3*$^{+/-}$/MMTV-PyMT males in either the FVB/C57BL/6 or C57BL/6 background. This mating strategy resulted in experimental female mice with an ~25% FVB and ~75% C57BL/6 genome (termed FVB/C57BL/6) or congenic C57BL/6 females, respectively. Genotypes were determined by PCR using the primers shown in Supplementary Table SI (Song et al. 2010) under the following reaction conditions: 94°C 2 min, 94°C 30 s, 58°C 45 s, 72°C 1 min, 72°C 10 min for 35 cycles. PCR products were analyzed on a 1.0% agarose gel. All experimental protocols pertaining to animal studies were approved by the Institute for Animal Studies of the Albert Einstein College of Medicine.

Antibodies and reagents

The following antibodies were used for western analyses at the concentrations indicated. Rabbit monoclonal anti-galectin-1 (EPR3205; 1/5000) and anti-galectin-8 (EPR4857; 1/5000) antibodies were from Epitomics (Burlingame, CA), rat monoclonal anti-galectin-3 (M3/38) (1/5000) antibody was prepared in conditioned medium from the M3/38 hybridoma line kindly provided by Dr. Timothy Springer (Harvard Medical School, Boston, MA) and guinea pig polyclonal anti-galectin-2 (1/2000) and rabbit polyclonal anti-galectin-4 (1/1000) antibodies were generous gifts from Dr. Junko Nio-Kobayashi (University of Hokkaido, Sapporo, Japan) (Nio-Kobayashi et al. 2009). Rabbit polyclonal anti-galectin-7 antibody (1/10,000) was purchased from Bethyl Laboratories (Montgomery, TX). Goat polyclonal anti-galectin-9 antibody (sc-19294; 1/500), rabbit polyclonal anti-phosphorylated FAK (Tyr925) (sc-11766-R; 1/500), anti-FAK (sc-557; 1/500) antibodies and donkey anti-goat IgG-horse radish peroxidase (HRP) secondary antibody (sc-2020; 1/2500) were from Santa Cruz Biotechnology (Dallas, TX). Mouse polyclonal anti-galectin-12 antibody (1/1000) and *Lgals12*$^{+/+}$ and *Lgals12*$^{-/-}$ adipose tissue lysates were gifts from Dr. Fu-Tong Liu (UC Davis School of Medicine, Davis, CA) (Yang et al. 2011). Rabbit anti-phosphorylated p44/42 MAPK (pERK1/2) (Thr202/Tyr204) (D13.14.4E) XP® (4370; 1/2000) and mouse anti-ERK1/2 monoclonal antibody (L34F12) (4696; 1/2000), rabbit polyclonal anti-phospho-Akt (Ser473) (9271; 1/1000), anti-Akt (9272; 1/1000), anti-phosphorylated p38 MAPK (Thr180/Tyr182) (9211; 1/500) and anti-p38MAPK (9212; 1/500) antibodies were purchased from Cell Signaling Technology (Danvers, MA). Mouse monoclonal anti-β-actin antibody (AC-15) (ab6276; 1/5000) was purchased from Abcam (Cambridge, MA). Rabbit polyclonal anti-phosphorylated Src (Tyr418) antibody (44660G; 1/500), anti-rabbit, anti-rat and anti-guinea pig IgG-HRP secondary antibodies (1/10,000) and Alexa Fluor 680 goat anti-mouse IgG-H + L (1/10,000) secondary antibodies were purchased from Life Technologies (Grand Island, NY). IRDye800-conjugated goat anti-rabbit IgG-H + L (1/10,000) was from Rockland Immunochemicals (Gilbertsville, PA). Anti-mouse IgG-HRP secondary antibody (1/10,000) was from Thermo Scientific (Rockford, IL). Mouse monoclonal anti-Src antibody (05-184; 1/500) was from Millipore (Billerica, MA). Biotinylated E-PHA, L-PHA, DSA and Streptavidin-HRP were from Vector Labs (Burlingame, CA). All chemicals were purchased from either Sigma-Aldrich (St. Louis, MO) or Thermo Fisher Scientific (Rockville, MD), unless indicated otherwise.

Tumor analysis

All 10 MG of each mouse were palpated twice a week, beginning at 6 weeks of age, and the date of the first palpable mass in each mammary gland was recorded. Both C57BL/6 and FVB/C57BL/6 cohorts were investigated simultaneously. Mice of 15–17 weeks (FVB/C57BL/6) or 19–20 weeks (C57BL/6) were euthanized and individual solid tumor masses were excised and weighed. Some tumors were used to establish TEC lines or frozen on dry ice and stored at −80°C for protein, DNA or RNA extraction.

Lung metastasis

Preliminary gross anatomical and histological examinations of lungs from MMTV-PyMT mice at ~20 weeks were performed by visual inspection of surface metastatic nodules of intact lung or by examination of three serial sections sampled at 100 μm intervals of paraffin-embedded lung tissue stained with hematoxylin and eosin. Lung metastasis was also investigated by real-time qPCR analysis of PyMT transcripts as described previously (Song et al. 2010) with some modifications. Briefly, total RNA was extracted from a whole lung in TRIzol (1 mL per 100 mg lung), treated with DNaseI (QIAGEN, Valencia, CA) and purified by RNA Protect mini kit (QIAGEN). The cDNA was synthesized as described (Song et al. 2010). Real-time PCR was performed in an iQ5 (Bio-Rad, Hercules, CA) with POWER SYBR green master mix (Life Technologies), the cDNA derived from 40 ng of original RNA material and the primers for PyMT and β-actin were as previously described (Song et al. 2010). ΔCt values were obtained by subtracting the Ct value of β-actin from that of PyMT in the same cDNA sample. The relative abundance of PyMT transcripts between two genotypes was compared by using the formula $(1/2^{(\Delta Ct(sample)-\Delta Ct(control))})$, in which ΔCt(sample) represents the ΔCt value of each cDNA sample and ΔCt (control) represents the sample with the highest ΔCt in the control group (also an overall highest). All reactions were run in duplicate in two independent experiments.

[^{18}F]Fluoro-2-deoxyglucose PET imaging

The mice were fasted overnight (18–20 h) and injected with 300–400 μCi (12–15 MBq) of [^{18}F] fluoro-2-deoxyglucose in 0.1 mL normal saline via the tail vein 1 h before imaging. The mice were secured to the imaging palette with a breathing tube affixed over their snout to supply 1.5% isoflurane–oxygen mixture anesthesia throughout the imaging portion of the procedure. Each mouse was placed on a heating pad before and during scanning to maintain normal body temperature. The mice were imaged by an Inveon Multimodality scanner (Siemens, Knoxville, TN) using its PET module. PET imaging is performed using the PET gantry, which provides a 12.7 cm axial and 10 cm transaxial active field of view. The PET scanner has no septa, and acquisitions are performed in the 3D list mode. A reconstructed full-width-half-max resolution of <1.4 mm is achievable in the center of the axial field of view. List mode acquisition of data is performed to permit dynamic re-framing for kinetic evaluation of the radiotracer uptake, where indicated. After each acquisition, data were sorted into 3D sinograms, and images were reconstructed using a two dimensional (2D)-Ordered Subset Expectation Maximization algorithm. Data were corrected for decay, dead time counting losses, random coincidences and the measured nonuniformity of detector response (i.e. normalized), but not for attenuation or scatter. Analysis was performed by using the ASIPRO software (Siemens). All image studies were inspected visually in a rotating 3D projection display to identify interpretability and image artifacts. Regions of interest (ROI) were manually defined around areas of individual MG with radiotracer uptake. Successive scrolling through 2D slices (each 1.2 mm thick in the axial images) permitted measurement of radioactivity within defined volumes. Corrected counts per cc within this volume divided by the counts per gram of total body mass of injected radioactivity determined the SUV. SUV_{max}, the maximum value of SUV within each tumor volume was determined in six mammary gland regions (a pair of first, second/third and fifth) per mouse, as shown in Figure 4. The second and third mammary gland regions were analyzed as one region, as it was often hard to distinguish the boundaries of tumors developed in that region. The fourth mammary gland was excluded as it was often overwrapped with hot spots resulting from radioactivity within the digestive tracts.

Cell culture

TECs were isolated from mouse mammary tumors as described (Song et al. 2010), and cells were passaged at least eight times and no >11 times. TECs were grown in growth medium (20% heat inactivated fetal bovine serum; Gemini, West Sacramento, CA), 1x penicillin/streptomycin (Life Technologies), 1.25 μg/mL Fungizone (Life Technologies), 20 ng/mL recombinant mouse EGF (Peprotech, Rocky Hill, NJ), 10 μg/mL insulin (Sigma-Aldrich or Gemini)/DMEM (Life Technologies; #11965) at 37°C, 5% CO_2.

Protein extraction, western and lectin blot analyses

About 30–100 mg solid tumors were mechanically homogenized in 300–1000 μl of tumor lysis buffer (10 mM Tris–HCl (pH 7.5), 300 mM lactose, 1 mM ethylenediaminetetraacetic acid (EDTA) and COMPLETE protease and PhosStop phosphatase inhibitors (Roche, Indianapolis, IN)). Homogenates were centrifuged at 1800 rpm for 10 min at 4°C and the supernatant was stored at −80°C. TEC lysates were prepared by scraping the cells off the culture plate in 250 μL/10 cm plate of TEC lysis buffer (50 mM Tris–HCl (pH 7.5), 150 mM NaCl, 1 mM EDTA, 1% Triton-X 100) with 300 mM lactose and 1× COMPLETE protease inhibitor (Roche). Lysates were microcentrifuged at 3000 rpm for 10 min at 4°C and the supernatant was stored at −80°C. As for control lysates, mouse small intestine lysates containing galectin-2 were prepared from C57BL/6 mouse as described (Nio-Kobayashi et al. 2009). Skin lysates containing galectin-7 were prepared by homogenizing the epidermis of C57BL/6 mice in TEC lysis buffer and microcentrifuged at 14,000 rpm for 15 min at 4°C. Protein concentration was measured by a Bio-Rad *DC* protein assay kit (Bio-Rad). For sodium dodecyl sulphate–polyacrylamide gel electrophoresis (SDS–PAGE) analysis, equal amounts of protein lysates (10–80 μg) were solubilized in SDS–PAGE loading buffer containing β-mercaptoethanol at 5% (final), heated at 95°C for 10 min and then separated on a 10, 12 or 15% SDS–PAGE gel along with molecular standards (Precision Plus Protein Dual Color Standards, Bio-Rad). Proteins were transferred to a Polyscreen polyvinylidene difluoride (PVDF) membrane (PerkinElmer, Waltham, MA) in Tris-glycine buffer containing 5% methanol, and western blot analysis was conducted as described previously (Song et al. 2010). Briefly, membranes were blocked in blocking buffer Tris-buffered saline and Tween 20 (TBS-T) (25 mM Tris–HCl, 150 mM NaCl, 0.05% Tween 20, pH 7.5) with either 3% bovine serum albumin (BSA) (for signaling molecules) or 3% nonfat dry milk (for all other antibodies) for over 1 h, and then incubated with primary antibody diluted in 3% Cold Fish Gelatin, 1% BSA, 0.001% Thimerosal/TBS-T at room

temperature for 1–3 h. After washing with TBS-T, membranes were incubated with HRP-conjugated secondary antibody diluted in the appropriate blocking buffer for 1 h. After washing with TBS-T, bands were visualized using an enhanced chemiluminescence (ECL) kit (Thermo Scientific) and exposed to film (Denville scientific, South Plainfield, NJ) and scanned or imaged with Fujifilm LAS-3000 (Valhalla, NY). When applicable, band intensity was quantified using NIH ImageJ (Bethesda, MD). For lectin blotting, membranes were blocked in 3% nonfat dry milk/TBS-T, incubated with biotinylated E-PHA, L-PHA or DSA (Vector Labs) at 10 or 15 µg/mL diluted in blocking buffer at room temperature for 1 h or overnight at 4°C. Membranes were washed with TBS-T, incubated with Streptavidin-HRP (1/5000; Vector Labs) for 1 h, washed with TBS-T and visualized using an ECL kit and exposed onto films.

RNA extraction and RT–PCR

Total RNA was extracted from ~50 mg of solid tumor by homogenization in 1 mL of TRIzol and purified according to the manufacturer's protocol. Residual genomic DNA was removed using a TURBO DNA-free kit (Life Technologies). For TEC, cells (80–90% confluent) were lysed in 500 µl (per 10 cm plate) of TRIzol. RNA was purified according to the manufacturer's protocol, followed by DNaseI treatment (QIAGEN) and purification using an RNA Protect mini kit (QIAGEN). The cDNA was synthesized using random hexamers and the SuperScript III first-strand synthesis system (Life Technologies). cDNA derived from 50 or 100 ng of RNA starting material was used as template with primers specific to each galectin gene or *Mgat3*, *Mgat5* and PyMT as described (Song et al. 2010) (Supplementary Table SII). Galectin primers were designed using the online program, Primer3 (Koressaar and Remm 2007; Untergasser et al. 2012). The following reaction conditions were used: 94°C 2 min, 94°C 30 s, 58°C 45 s, 72°C 1 min, 72°C 10 min for 30–35 cycles. PCR products were visualized on 1 or 2% agarose gels.

Signaling assays in TECs

TECs (85–90% confluent in 24-well plates) were serum-starved for 24 h and stimulated with 50 ng/mL of recombinant mouse EGF (R&D Systems, Minneapolis, MN) at 37°C for the indicated times. To terminate the reaction, plates were placed on an ice slurry, and then washed once with 1 mL ice-cold phosphate-buffered saline (PBS), pH 7.2, lysed in 2× SDS–PAGE buffer diluted with TEC lysis buffer containing COMPLETE protease and PhosStop phosphatase inhibitors (Roche), incubated at 95°C for 10 min and then electrophoresed on 12% SDS–PAGE gels and transferred to PVDF membranes. Membranes were blocked in Odyssey blocking buffer and then incubated with rabbit anti-phosphorylated p44/42 MAPK (pERK1/2) antibody (Thr202/Tyr204) and mouse anti-ERK1/2 mAb (L34F12) in blocking buffer at 4°C overnight. Following washes with PBS/0.025% Tween-20 (PBS-T), pH 7.2, IRDye800-conjugated goat anti-rabbit IgG-H + L and Alexa Fluor 680 goat anti-mouse IgG-H + L diluted in blocking buffer were added for 1 h at room temperature, the membranes were washed with PBS-T, rinsed with PBS and bands were visualized and quantified by the ODYSSEY IR Imaging System (LI-COR BioSciences, Lincoln, NE).

LGALS and MGAT gene expression data from human breast cancer databases

Gene expression profiles of breast tumors with matched exome sequencing data ($n = 466$) were obtained from the TCGA study (Network CGA 2012). These included 81 basal-like, 53 HER2, 210 Luminal A, 114 Luminal B and 8 Normal-like tumors. Samples assigned to the Normal-like subtype were excluded as they are believed to be substantially contaminated by normal tissue. Because the TCGA data lack extensive clinical follow-up, we examined additional datasets (van de Vijver et al. 2002; Wang et al. 2005; Gyorffy et al. 2010) to test for association between our genes of interest and patient outcomes. KM plotter was used to analyze RFS in breast cancer patients (Gyorffy et al. 2010). Where multiple Affymetrix probes were available for a given gene, the optimal probe was selected using Jetset (Li et al. 2011).

Statistical analysis

Statistical analyses of experimental data were performed using either GraphPad Prism (La Jolla, CA) or the Microsoft® Excel software (Redmond, WA).

Supplementary Data

Supplementary data for this article are available online at http://glycob.oxfordjournals.org/.

Funding

This work was supported by the National Institutes of Health (RO1 CA30645, RO1 CA36434) to P.S. and (T32CA009173) to H.E. M.; the American Cancer Society (RSG-TBE-123001) to P.A.K.; Susan G. Komen for the Cure (KG091136) to O.G. Partial support was provided by the National Institutes of Health Cancer Center grant (PO1 13330) to P.S., P.A.K. and to E.J.F. and W.R.K. of the Einstein MicroPET Core Laboratory.

Acknowledgements

We thank all those mentioned in the Materials and methods section for mouse strains and reagents, members of the Pamela Stanley laboratory and Dr. Linda A Jelicks for helpful suggestions and Huimin Shang and Subha Sundaram for excellent technical assistance.

Abbreviations

AKT, Protein kinase B; BLBC, Basal-like breast cancer; BSA, bovine serum albumin; CHO, Chinese hamster ovary; CRD, Carbohydrate recognition domain; DSA, *Datura stramonium* agglutinin; ECL, enhanced chemiluminescence; EDTA: ethylenediaminetetraacetic acid; EGF, epidermal growth factor; E-PHA, *Phaseolus vulgaris* erythroagglutinin; ER, estrogen receptor; ERK, Extracellular signal-regulated kinase; FAK, focal adhesion kinase; FVB, FVB/N; GlcNAc, N-acetylglucosamine; GLUT1, Glucose transporter 1; HER2, human epidermal growth factor

receptor 2; HR, hazard ratio; HRP, horse radish peroxidase; KM, Kaplan–Meier; LacNAc, N-acetyllactosamine; L-PHA, *Phaseolus vulgaris* leukoagglutinin; MG, mammary glands; MGAT, N-glycan branching GalNAc transferase; microPET, micro positron emission tomography; MMTV, mouse mammary tumor virus; NKI-295, 295 breast cancer patients of Netherlands Cancer Institute; p38MAPK, p38 mitogen-activated protein kinase; PBS, phosphate-buffered saline; PET, positron emission tomography; PVDF, polyscreen polyvinylidene difluoride; PyMT, Polyoma middle T antigen; RFS, relapse-free survival; ROI, Regions of interest; RT–PCR, reverse transcription–polymerase chain reaction; SDS–PAGE: sodium dodecyl sulphate–polyacrylamide gel electrophoresis; SEM, standard error of mean; SUV, standardized-uptake value; TBS, Tris-buffered saline; TCGA, The Cancer Genome Atlas; TEC, tumor epithelial cell; UDP, uridine diphosphate.

References

Ahmad N, Gabius HJ, Andre S, Kaltner H, Sabesan S, Roy R, Liu B, Macaluso F, Brewer CF. 2004. Galectin-3 precipitates as a pentamer with synthetic multivalent carbohydrates and forms heterogeneous cross-linked complexes. *J Biol Chem*. 279:10841–10847.

Andre S, Kozar T, Schuberth R, Unverzagt C, Kojima S, Gabius HJ. 2007. Substitutions in the N-glycan core as regulators of biorecognition: The case of core-fucose and bisecting GlcNAc moieties. *Biochemistry.* 46:6984–6995.

Andre S, Unverzagt C, Kojima S, Frank M, Seifert J, Fink C, Kayser K, von der Lieth CW, Gabius HJ. 2004. Determination of modulation of ligand properties of synthetic complex-type biantennary N-glycans by introduction of bisecting GlcNAc in silico, in vitro and in vivo. *Eur J Biochem*. 271: 118–134.

Banh A, Zhang J, Cao H, Bouley DM, Kwok S, Kong C, Giaccia AJ, Koong AC, Le QT. 2011. Tumor galectin-1 mediates tumor growth and metastasis through regulation of T-cell apoptosis. *Cancer Res*. 71:4423–4431.

Basu GD, Pathangey LB, Tinder TL, Lagioia M, Gendler SJ, Mukherjee P. 2004. Cyclooxygenase-2 inhibitor induces apoptosis in breast cancer cells in an in vivo model of spontaneous metastatic breast cancer. *Mol Cancer Res*. 2:632–642.

Berger T, Cheung CC, Elia AJ, Mak TW. 2010. Disruption of the Lcn2 gene in mice suppresses primary mammary tumor formation but does not decrease lung metastasis. *Proc Natl Acad Sci USA*. 107:2995–3000.

Boscher C, Dennis JW, Nabi IR. 2011. Glycosylation, galectins and cellular signaling. *Curr Opin Cell Biol*. 23:383–392.

Brewer CF, Miceli MC, Baum LG. 2002. Clusters, bundles, arrays and lattices: Novel mechanisms for lectin-saccharide-mediated cellular interactions. *Curr Opin Struct Biol*. 12:616–623.

Brisson JR, Carver JP. 1983. Solution conformation of asparagine-linked oligosaccharides: Alpha(1–2)-, alpha(1–3)-, beta(1–2)-, and beta(1–4)-linked units. *Biochemistry.* 22:3671–3680.

Campbell C, Stanley P. 1984. A dominant mutation to ricin resistance in Chinese hamster ovary cells induces UDP-GlcNAc:glycopeptide beta-4-N-acetylglucosaminyltransferase III activity. *J Biol Chem*. 259:13370–13378.

Cramer EP, Glenthoj A, Hager M, Juncker-Jensen A, Engelholm LH, Santoni-Rugiu E, Lund LR, Laerum OD, Cowland JB, Borregaard N. 2012. No effect of NGAL/lipocalin-2 on aggressiveness of cancer in the MMTV-PyMT/FVB/N mouse model for breast cancer. *PLoS One*. 7:e39646.

Croci DO, Salatino M, Rubinstein N, Cerliani JP, Cavallin LE, Leung HJ, Ouyang J, Ilarregui JM, Toscano MA, Domaica CI, et al. 2012. Disrupting galectin-1 interactions with N-glycans suppresses hypoxia-driven angiogenesis and tumorigenesis in Kaposi's sarcoma. *J Exp Med*. 209:1985–2000.

Dalotto-Moreno T, Croci DO, Cerliani JP, Martinez-Allo VC, Dergan-Dylon S, Mendez- Huergo SP, Stupirski JC, Mazal D, Osinaga E, Toscano MA,, et al. 2013. Targeting galectin-1 overcomes breast cancer-associated immunosuppression and prevents metastatic disease. *Cancer Res*. 73:1107–1117.

Davie SA, Maglione JE, Manner CK, Young D, Cardiff RD, MacLeod CL, Ellies LG. 2007. Effects of FVB/NJ and C57Bl/6J strain backgrounds on mammary tumor phenotype in inducible nitric oxide synthase deficient mice. *Transgenic Res*. 16:193–201.

Dennis JW, Brewer CF. 2013. Density-dependent lectin-glycan interactions as a paradigm for conditional regulation by posttranslational modifications. *Mol Cell Proteomics*. 12:913–920.

Dennis JW, Lau KS, Demetriou M, Nabi IR. 2009. Adaptive regulation at the cell surface by N-glycosylation. *Traffic*. 10:1569–1578.

Di Lella S, Sundblad V, Cerliani JP, Guardia CM, Estrin DA, Vasta GR, Rabinovich GA. 2011. When galectins recognize glycans: From biochemistry to physiology and back again. *Biochemistry.* 50:7842–7857.

Eude-Le Parco I, Gendronneau G, Dang T, Delacour D, Thijssen VL, Edelmann W, Peuchmaur M, Poirier F. 2009. Genetic assessment of the importance of galectin- 3 in cancer initiation, progression, and dissemination in mice. *Glycobiology.* 19:68–75.

Gatenby RA, Gillies RJ. 2004. Why do cancers have high aerobic glycolysis? *Nat Rev Cancer*. 4:891–899.

Guo H, Nairn A, dela Rosa M, Nagy T, Zhao S, Moremen K, Pierce M. 2012. Transcriptional regulation of the protocadherin beta cluster during Her-2 protein- induced mammary tumorigenesis results from altered N-glycan branching. *J Biol Chem*. 287:24941–24954.

Guy CT, Cardiff RD, Muller WJ. 1992. Induction of mammary tumors by expression of polyomavirus middle T oncogene: A transgenic mouse model for metastatic disease. *Mol Cell Biol*. 12:954–961.

Gyorffy B, Lanczky A, Eklund AC, Denkert C, Budczies J, Li Q, Szallasi Z. 2010. An online survival analysis tool to rapidly assess the effect of 22,277 genes on breast cancer prognosis using microarray data of 1,809 patients. *Breast Cancer Res Treat*. 123:725–731.

Haga Y, Ishii K, Suzuki T. 2011. N-glycosylation is critical for the stability and intracellular trafficking of glucose transporter GLUT4. *J Biol Chem*. 286: 31320–31327.

Houzelstein D, Goncalves IR, Orth A, Bonhomme F, Netter P. 2008. Lgals6, a 2-million- year-old gene in mice: A case of positive Darwinian selection and presence/absence polymorphism. *Genetics*. 178:1533–1545.

Irie A, Yamauchi A, Kontani K, Kihara M, Liu D, Shirato Y, Seki M, Nishi N, Nakamura T, Yokomise H., et al. 2005. Galectin-9 as a prognostic factor with antimetastatic potential in breast cancer. *Clin Cancer Res*. 11: 2962–2968.

Iyengar P, Espina V, Williams TW, Lin Y, Berry D, Jelicks LA, Lee H, Temple K, Graves R, Pollard J., et al. 2005. Adipocyte-derived collagen VI affects early mammary tumor progression in vivo, demonstrating a critical interaction in the tumor/stroma microenvironment. *J Clin Invest*. 115:1163–1176.

Joyce JA, Pollard JW. 2009. Microenvironmental regulation of metastasis. *Nat Rev Cancer*. 9:239–252.

Kitagawa T, Tsuruhara Y, Hayashi M, Endo T, Stanbridge EJ. 1995. A tumor-associated glycosylation change in the glucose transporter GLUT1 controlled by tumor suppressor function in human cell hybrids. *J Cell Sci*. 108(Pt 12):3735–3743.

Koressaar T, Remm M. 2007. Enhancements and modifications of primer design program Primer3. *Bioinformatics*. 23:1289–1291.

Landskroner-Eiger S, Qian B, Muise ES, Nawrocki AR, Berger JP, Fine EJ, Koba W, Deng Y, Pollard JW, Scherer PE. 2009. Proangiogenic contribution of adiponectin toward mammary tumor growth in vivo. *Clin Cancer Res*. 15:3265–3276.

Lau KS, Dennis JW. 2008. N-Glycans in cancer progression. *Glycobiology.* 18:750–760.

Lau KS, Partridge EA, Grigorian A, Silvescu CI, Reinhold VN, Demetriou M, Dennis JW. 2007. Complex N-glycan number and degree of branching cooperate to regulate cell proliferation and differentiation. *Cell*. 129: 123–134.

Leffler H, Carlsson S, Hedlund M, Qian Y, Poirier F. 2004. Introduction to galectins. *Glycoconj J*. 19:433–440.

Li Q, Birkbak NJ, Gyorffy B, Szallasi Z, Eklund AC. 2011. Jetset: Selecting the optimal microarray probe set to represent a gene. *BMC Bioinform*. 12:474.

Miwa HE, Song Y, Alvarez R, Cummings RD, Stanley P. 2012. The bisecting GlcNAc in cell growth control and tumor progression. *Glycoconj J*. 29: 609–618.

Network CGA. 2012. Comprehensive molecular portraits of human breast tumours. *Nature*. 490:61–70.

Nio-Kobayashi J, Takahashi-Iwanaga H, Iwanaga T. 2009. Immunohistochemical localization of six galectin subtypes in the mouse digestive tract. *J Histochem Cytochem*. 57:41–50.

Nobumoto A, Nagahara K, Oomizu S, Katoh S, Nishi N, Takeshita K, Niki T, Tominaga A, Yamauchi A, Hirashima M. 2008. Galectin-9 suppresses tumor metastasis by blocking adhesion to endothelium and extracellular matrices. *Glycobiology.* 18:735–744.

North SJ, Huang HH, Sundaram S, Jang-Lee J, Etienne AT, Trollope A, Chalabi S, Dell A, Stanley P, Haslam SM. 2010. Glycomics profiling of Chinese hamster ovary cell glycosylation mutants reveals N-glycans of a novel size and complexity. *J Biol Chem*. 285:5759–5775.

Ohtsubo K, Takamatsu S, Minowa MT, Yoshida A, Takeuchi M, Marth JD. 2005. Dietary and genetic control of glucose transporter 2 glycosylation promotes insulin secretion in suppressing diabetes. *Cell*. 123:1307–1321.

Partridge EA, Le Roy C, Di Guglielmo GM, Pawling J, Cheung P, Granovsky M, Nabi IR, Wrana JL, Dennis JW. 2004. Regulation of cytokine receptors by Golgi N-glycan processing and endocytosis. *Science*. 306:120–124.

Patnaik SK, Potvin B, Carlsson S, Sturm D, Leffler H, Stanley P. 2006. Complex N- glycans are the major ligands for galectin-1, -3, and -8 on Chinese hamster ovary cells. *Glycobiology*. 16:305–317.

Priatel JJ, Sarkar M, Schachter H, Marth JD. 1997. Isolation, characterization and inactivation of the mouse Mgat3 gene: The bisecting N-acetylglucosamine in asparagine-linked oligosaccharides appears dispensable for viability and reproduction. *Glycobiology*. 7:45–56.

Seelenmeyer C, Stegmayer C, Nickel W. 2008. Unconventional secretion of fibroblast growth factor 2 and galectin-1 does not require shedding of plasma membrane- derived vesicles. *FEBS Lett*. 582:1362–1368.

Seelenmeyer C, Wegehingel S, Tews I, Kunzler M, Aebi M, Nickel W. 2005. Cell surface counter receptors are essential components of the unconventional export machinery of galectin-1. *J Cell Biol*. 171:373–381.

Song Y, Aglipay JA, Bernstein JD, Goswami S, Stanley P. 2010. The bisecting GlcNAc on N-glycans inhibits growth factor signaling and retards mammary tumor progression. *Cancer Res*. 70:3361–3371.

Stanley P, Caillibot V, Siminovitch L. 1975. Selection and characterization of eight phenotypically distinct lines of lectin-resistant Chinese hamster ovary cell. *Cell*. 6:121–128.

Thijssen VL, Barkan B, Shoji H, Aries IM, Mathieu V, Deltour L, Hackeng TM, Kiss R, Kloog Y, Poirier F., et al. 2010. Tumor cells secrete galectin-1 to enhance endothelial cell activity. *Cancer Res*. 70: 6216–6224.

Thijssen VL, Postel R, Brandwijk RJ, Dings RP, Nesmelova I, Satijn S, Verhofstad N, Nakabeppu Y, Baum LG, Bakkers J., et al. 2006. Galectin-1 is essential in tumor angiogenesis and is a target for antiangiogenesis therapy. *Proc Natl Acad Sci USA*. 103:15975–15980.

Untergasser A, Cutcutache I, Koressaar T, Ye J, Faircloth BC, Remm M, Rozen SG. 2012. Primer3–new capabilities and interfaces. *Nucleic Acids Res*. 40:e115.

van de Vijver M. 2005. Gene-expression profiling and the future of adjuvant therapy. *Oncologist*. 10 Suppl 2:30–34.

van de Vijver MJ, He YD, van't Veer LJ, Dai H, Hart AA, Voskuil DW, Schreiber GJ, Peterse JL, Roberts C, Marton MJ., et al. 2002. A gene-expression signature as a predictor of survival in breast cancer. *N Engl J Med*. 347:1999–2009.

Varki A, Cummings RD, Esko JD, Freeze HH, Stanley P, Bertozzi CR, Hart GW, Etlzler ME. 2009. *Essentials of Glycobiology*. 2nd edition Cold Spring Harbor laboratory Press: New York, NY.

Wang Y, Klijn JG, Zhang Y, Sieuwerts AM, Look MP, Yang F, Talantov D, Timmermans M, Meijer-van Gelder ME, Yu J., et al. 2005. Gene-expression profiles to predict distant metastasis of lymph-node-negative primary breast cancer. *Lancet*. 365:671–679.

Wang H, Yang H, Shivalila CS, Dawlaty MM, Cheng AW, Zhang F, Jaenisch R. 2013. One-step generation of mice carrying mutations in multiple genes by CRISPR/Cas-mediated genome engineering. *Cell*. 153:910–918.

Warburg O, Wind F, Negelein E. 1927. The metabolism of tumors in the body. *J Gen Physiol*. 8:519–530.

Williams TM, Medina F, Badano I, Hazan RB, Hutchinson J, Muller WJ, Chopra NG, Scherer PE, Pestell RG, Lisanti MP. 2004. Caveolin-1 gene disruption promotes mammary tumorigenesis and dramatically enhances lung metastasis in vivo. Role of Cav-1 in cell invasiveness and matrix metalloproteinase (MMP-2/9) secretion. *J Biol Chem*. 279:51630–51646.

Yang RY, Yu L, Graham JL, Hsu DK, Lloyd KC, Havel PJ, Liu FT. 2011. Ablation of a galectin preferentially expressed in adipocytes increases lipolysis, reduces adiposity, and improves insulin sensitivity in mice. *Proc Natl Acad Sci USA*. 108:18696–18701.

Ying H, Kimmelman AC, Lyssiotis CA, Hua S, Chu GC, Fletcher-Sananikone E, Locasale JW, Son J, Zhang H, Coloff JL., et al. 2012. Oncogenic Kras maintains pancreatic tumors through regulation of anabolic glucose metabolism. *Cell*. 149:656–670.

Young CD, Lewis AS, Rudolph MC, Ruehle MD, Jackman MR, Yun UJ, Ilkun O, Pereira R, Abel ED, Anderson SM. 2011. Modulation of glucose transporter 1 (GLUT1) expression levels alters mouse mammary tumor cell growth in vitro and in vivo. *PLoS One*. 6:e23205.